



Synthesis, spectral and electrochemical properties of selected boron ketiminates with aminocoumarin fragment

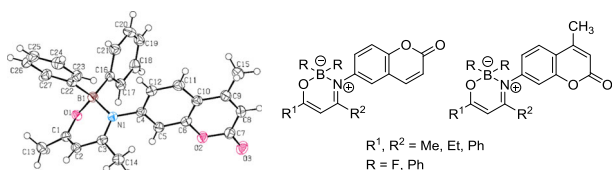
Hana Doušová¹ · Numan Almonasy¹ · Tomáš Mikysek² · Jiří Váňa¹ · Miloš Nepraš¹ · Božena Frumarová³ · Miroslav Dvořák⁴ · Zdeňka Růžičková⁵ · Petr Šimůnek¹ 

Received: 27 March 2018 / Accepted: 24 June 2018
© Springer-Verlag GmbH Austria, part of Springer Nature 2018

Abstract

Six novel oxazaborines based on 7-aminocoumarin substituted by either fluoride or phenyl group on the boron atom were prepared from the corresponding enaminones. The compounds were characterized by means of ¹H, ¹³C, ¹⁹F, and ¹¹B NMR in solution, X-ray diffraction in crystal, UV–Vis spectroscopy, and electrochemistry. The observed optical properties were compared to the DFT calculations. Dynamic behaviour of selected oxazaborines was studied by means of ¹⁹F and ¹H VT NMR and 2D EXSY. Both the enaminones and oxazaborines exhibit relatively strong fluorescence both in solid state and in frozen 2-methyltetrahydrofuran at 77 K, but none in solution. In some cases, phosphorescence was observed as well. Preliminary aggregation tests revealed aggregation induced emission (AIE) properties of the studied molecules. Concerning the electrochemical properties, the first reduction of all the oxazaborines studied proceeds as transport controlled one-electron (quasi)reversible process whereas the first oxidation of BPh₂ oxazaborines proceeds as a two-electron irreversible process most probably of the ECE type. The oxidation of BF₂ compounds was not possible to obtain within the given potential window. Analysis of frontier orbitals showed that change from BF₂ to BPh₂ leads to decrease of energy gap.

Graphical abstract



Electronic supplementary material The online version of this article (<https://doi.org/10.1007/s00706-018-2262-3>) contains supplementary material, which is available to authorized users.

✉ Petr Šimůnek
petr.simunek@upce.cz

- ¹ Faculty of Chemical Technology, Institute of Organic Chemistry and Technology, University of Pardubice, Studentská 573, 532 10 Pardubice, Czech Republic
- ² Department of Analytical Chemistry, Faculty of Chemical Technology, University of Pardubice, Studentská 573, 532 10 Pardubice, Czech Republic
- ³ Institute of Macromolecular Chemistry, Czech Academy of Sciences, v.v.i., Heyrovského nám. 2, 162 06 Prague, Czech Republic

- ⁴ Department of Physical Electronics, Faculty of Nuclear Sciences and Physical Engineering, Czech Technical University, V Holešovičkách 2, 180 00 Prague, Czech Republic
- ⁵ Department of General and Inorganic Chemistry, Faculty of Chemical Technology, University of Pardubice, Studentská 573, 532 10 Pardubice, Czech Republic

Keywords Enaminones · NMR spectroscopy · X-ray structure determination · Fluorescence · UV/Vis spectroscopy · AIE · Electrochemistry

Introduction

Due to the still growing area of the applicability of luminescent molecules, the searching for novel luminophores is an actual topic. One approach is to combine known luminophores into one molecule [1]. In our present research we have combined two well-known luminophores: aminocoumarins and boron ketiminates. 7-Aminocoumarins are excellent luminophores, exhibiting high fluorescence quantum yields and large Stokes shifts [2–13]. From huge amount of applications and studies on 7-aminocoumarins that can be found in the literature see, e.g., [14–33].

An advantage of coumarins is the possibility of adding other substituents that both affects their spectral characteristics and enables their interaction with an environment which is important for their applications [10, 34–37]. Spectral characteristics of 7-aminocoumarins can be especially affected by the substitution on the nitrogen [2]. Series of papers describing the relationship between the structure and luminescence properties of coumarin dyes was published by Cole et al. [1, 38, 39].

Difluoroboron complexes of β -enaminones **I** (Fig. 1) which belong to the family of β -iminoenolate boron complexes [40] have recently attracted attention as a promising class of fluorophores. Number of them have been synthesized and characterized [40–73] showing interesting AIE (aggregation-induced emission) [48–50, 59, 61, 62, 64, 66, 70, 74–77] as well as MLC (mechanoluminescent chromism) [48–50, 74, 75, 78] properties. An important part of this class of compounds form salicylaldimine-

derived complexes (boranils) **II** [51, 53, 55, 78] and fused boron complexes **III** where nitrogen originates from annelated heterocyclic ring [43, 45, 57, 59, 60, 75, 79–90]. In contrast to their difluoro analogues, diarylboron chelates of β -enaminones are less characterized [68, 91–94]. During the past several years our group has published synthesis, NMR and X-ray characterization, basic fluorescence and DSC study and some interesting chemical behaviour for number of 2,2-diphenyl-1,3,2-oxazaborines, prepared from β -enaminones and related compounds [41, 95–97]. Recently [98] we have synthesized and characterized (NMR, X-ray) several boron iminoenolates **IV** having coumarin-6-yl fragment on their nitrogen atom (Fig. 1). We have also performed introductory study of their fluorescence properties. The compounds exhibited fluorescence in solid state as well as in frozen 2-methyltetrahydrofuran at 77 K. Exploratory tests showed promising AIE properties of the tested compounds. AIE-active coumarin-based boron complexes have been recently published [76].

As 7-aminocoumarins are better fluorophores than their 6-amino relatives [99] it inspired us to prepare, characterize, and explore fluorescence and electrochemical behaviour of boron iminoenolates **V** (Fig. 1) substituted with coumarin-7-yl fragment on the nitrogen atom. We used 7-amino-4-methylcoumarin derivative as it is better synthetically accessible than the corresponding 4-unsubstituted one, although C4-methyl group can, in principle, have some effect on the properties studied. Another goal of this work is to compare the properties of 7-aminocoumarin derivatives **V** with their 6-aminocoumarin analogues **IV** as well as study of the effect of the coumarin fragment. For this purpose, iminoenolates with *N*-Me fragment were also prepared and studied.

Results and discussion

Synthesis of boron ketiminates

The starting β -enaminones **3** were prepared using classic condensation of corresponding β -diketone **2** with appropriate amine (7-amino-4-methylcoumarin (**1a**), methylamine (**1b**), or 6-aminocoumarin (**1c**) [98], resp.) (Scheme 1). Enaminones **3** were converted to the corresponding oxazaborines **4**, **5** upon reaction with compounds of trivalent boron (BPh₃ or BF₃·Et₂O, resp.) (Scheme 1).

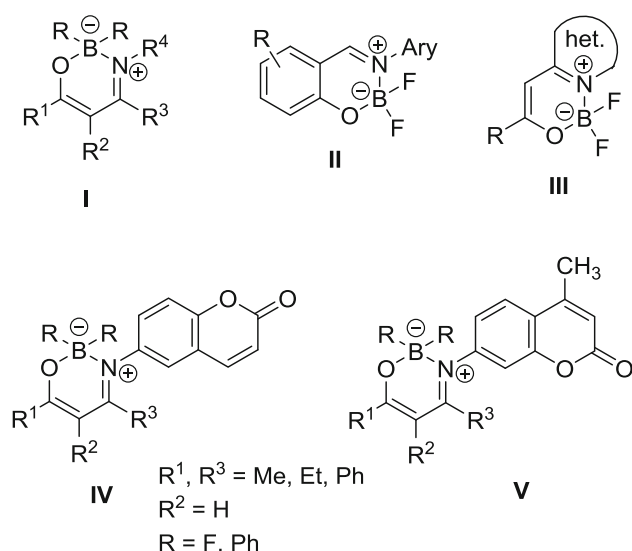
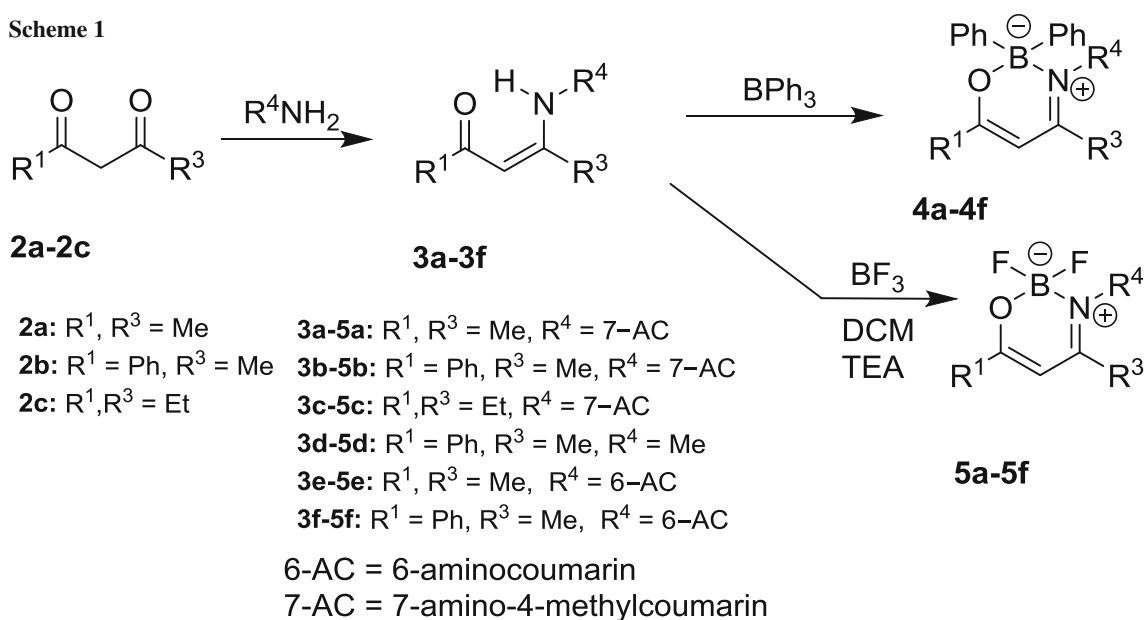


Fig. 1 General formulae of relevant boron iminoenolates

Scheme 1



NMR spectroscopy of the boron ketiminates

¹⁹F NMR spectra of ketiminates **5** reflect their dynamics. The dynamics is both solvent and temperature dependent. At laboratory temperature in CDCl₃ ¹⁹F NMR spectra of compounds **5a**, **5b** (Fig. S28) consist of one broad signal indicating relatively fast exchange of both the fluorines (are equivalent on the NMR time scale). No boron splitting is observable due to the broadening. The structure and reactivity of compound **5d** was previously studied by Itoh et al. [100–103] where authors, on the basis of ¹⁹F NMR splitting, concluded on the non-equivalency of the fluorines. The fluorines in compound **5d** (lacking the coumarin fragment) give sharp signal consisting of 1:1:1:1 lines with distances 16.7 Hz (¹J(¹⁹F, ¹¹B)) which is comparable with those observed for similar compounds [98, 100] (Fig. S28). However, our interpretation, based on both ¹⁹F VT NMR and boron-11 NMR properties (for details see Ref. [98]) is different from the one given in Ref. [100]. The fluorines in **5d** are equivalent even at laboratory temperature and the splitting 1:1:1:1 is due to boron-11 splitting. The sharp lines in the fluorine signal in ¹⁹F NMR spectrum of **5d** suggests higher rates of interconversion between the fluorines in comparison with **5a**, **5b**. The interconversion in **5a**, **5b** is slower than in **5d**, which could be due to the much different size of N-substituents (4-methylcoumarin-7-yl vs. methyl). The spectrum of compound **5c** is different from other compounds **5** (Fig. S28). Both the fluorines are non-equivalent and the spectrum looks like a broad AB-system (only the fluorine splitting is observable). This indicates that the exchange between the fluorines is slow on the

NMR time scale (the slowest from all compounds **5**). For comparison of all the fluorine spectra see Fig. S28.

The difference in the dynamic behaviour between compounds **5a–5c** and **5d** could be ascribed by the different size of the N-substituent. Considerably smaller methyl group enables much faster interconversion of the fluorines (free C–N rotation) in comparison with the 4-methylcoumarin-7-yl fragment (coalescence point for **5d** lies below 180 K). The size of the aminocoumarin fragment slows down the C–N rotation and makes it hindered with possible contributions of various conformers (especially flat and twisted form). Only a slight lowering the temperature makes both the fluorines clearly distinct and both geminal [²J(¹⁹F, ¹⁹F)] and one bond [¹J(¹⁹F, ¹¹B)] couplings are clearly visible (see Fig. S29). In accordance with this, an increasing the temperature leads to a gradual equivalency of the fluorines, where finally only boron splitting is observable (Fig. S29). Fluorine-19 NMR parameters of the compounds studied are summarized in Table 1.

The appearance of the boron-11 spectrum depends on the type of the oxazaborine. Signals of 2,2-difluoro derivatives **5** are split into triplets via direct boron–fluorine coupling with ¹J(¹¹B, ¹⁹F) = 14.6–15.2 Hz. The chemical shifts and coupling constants of **5** are comparable to those found for 6-aminocoumarin analogues [98]. The change of the N-substituent (**5a–5c**, → **5d**) has some effect on both the chemical shift and the coupling constant (Table 1). On the other hand, the boron signals of 2,2-diphenyl derivatives **4** are broad singlets. This is typical behaviour for this kind of compounds [95–98]. Chemical shifts are downfielded in

Table 1 ^{19}F and ^{11}B NMR parameters of compounds **4**, **5** in CDCl_3 at laboratory temperature

^{19}F	^{11}B
4a	5.49 br
4b	5.73 br
4c	5.21 br
4d	4.75 br
5a – 134.9, br s	0.34 (t, $^1J(^{11}\text{B}, ^{19}\text{F}) = 15.1$ Hz)
5b – 135.4, br s	0.68 (t, $^1J(^{11}\text{B}, ^{19}\text{F}) = 14.6$ Hz)
5c – 135.6 br d, – 134.3 br d	0.40 (t, $^1J(^{11}\text{B}, ^{19}\text{F}) = 15.2$ Hz)
5d – 140.0 (q 1:1:1:1)	0.74 (t, $^1J(^{11}\text{B}, ^{19}\text{F}) = 16.7$ Hz)
	$^1J(^{19}\text{F}, ^{11}\text{B}) = 16.7$ Hz
5e^a – 134.0 br s, – 135.6 br s	0.36 (t, $^1J(^{11}\text{B}, ^{19}\text{F}) = 15.2$ Hz)
5f^a – 134.5 br s, – 136.3 br s	0.68 (t, $^1J(^{11}\text{B}, ^{19}\text{F}) = 14.6$ Hz)

^aData taken from Ref. [98]

comparison with their BF_2 analogues, similarly to those described in [98] which is common [104].

Upon comparison of the proton and carbon chemical shifts of the atoms being most affected by the formation of the oxazaborine motif in **3** with those in **4**, **5** (Table 2), some conclusions can be drawn.

The formation of the oxazaborine ring causes downfield shift for proton H2 both in BF_2 and, to a lesser extent, BPh_2 derivatives. The change is practically homogeneous ($\Delta\delta = 0.29$ – 0.31 ppm for BF_2 and 0.18 – 0.19 ppm for BPh_2 , see Table 2, column 3) excepting **5d**, where H2 proton is slightly more downfielded ($\Delta\delta = 0.37$ ppm). Generally, the deshielding of H2 could be attributed to electron-withdrawing effect of the positively charged nitrogen and fluorines (in the case of **5**). For more detailed discussion see Ref. [100].

The upfield change of the C1 chemical shift can be ascribed to the coordination of the boron species leading to the change in the C–O bond order (from carbonyl to enol). The change is relatively significant ($\Delta\delta = -14$ to -19 ppm, see Table 2, column 5). Contrary to this, carbon C3 shows downfield shift due to the positively charged nitrogen (Table 2, column 9). These changes in C1/C3 shielding can be attributed to the fact, that enol-imino form is the more contributing (Fig. 2). This is similar to 6-aminocoumarin analogues studied previously [98]. Anomalous change of $\delta(\text{C3})$ in compounds **4d**, **5d** may be caused by the different electronic nature of the adjacent N-substituent (+ I effect compensating the positive charge at the nitrogen atom). Most of the data in Table 2 are consistent with those published in Ref. [100]. Generally, compounds **4** and **5** are similar to their 6-aminocoumarin analogues studied previously [98].

Both proton and carbon NMR spectra of compounds **4** also reflect their dynamics. Carbon spectrum of BPh_2 fragment of compound **4c** consists of two sets of signals that were undoubtedly assigned by means of 2D ^1H - ^{13}C HSQC (for the spectra see Supporting Info Figs. S19, S26; the signal of the quaternary C–B carbon is missing probably due to its broadness caused by the quadrupole effect of the adjacent boron atom). It indicates non-equivalency of the phenyls within of the BPh_2 fragment that can be explained by a deformed envelope structure of the oxazaborine ring with a slow interconversion between the phenyls on the NMR time scale. The envelope structure was confirmed by means of X-ray in the case of **4a** (see Figs. 3, S34). Similar features, albeit not so striking, can be seen in carbon spectra of **4a**, **4b** (signals of the relevant carbons are not fully separated, but broadened, see Supporting Info, Figs. S15a, S17a). The dynamics of compound **4c** is evident also on looking at proton NMR spectra measured in

Table 2 The chemical shifts and changes in the shielding of selected protons and carbons upon forming the oxazaborine ring

	$\delta(\text{H2})$	$\Delta\delta(\text{H2})$	$\delta(\text{C1})$	$\Delta\delta(\text{C1})$	$\delta(\text{C2})$	$\Delta\delta(\text{C2})$	$\delta(\text{C3})$	$\Delta\delta(\text{C3})$
3a	5.30		197.6		100.4		158.2	
5a	5.61	0.31	178.8	– 18.8	99.3	– 1.1	171.7	13.5
4a	5.48	0.18	180.2	– 17.4	100.8	0.4	169.1	10.9
3b	5.99		189.7		96.8		160.2	
5b	6.28	0.29	172.3	– 17.4	96.1	– 0.7	171.9	11.7
4b	6.18	0.19	173.3	– 16.4	97.7	0.9	169.7	9.5
3c	5.33		201.6		97.4		163.7	
5c	5.63	0.30	183.3	– 18.3	95.7	– 1.7	176.4	12.7
4c	5.51	0.18	184.5	– 17.1	97.2	– 0.2	174.0	10.3
3d^a	5.66		187.4		91.8		165.8	
5d	6.03	0.37	171.4	– 16.0	95.7	3.9	168.9	3.1
4d	5.84	0.18	170.2	– 17.2	96.6	4.8	168.9	3.1

^aFrom Ref. [107]

plane defined by the C1, C2, C3, and O1 atoms. Surprisingly, only the C–H···O short contacts are responsible for the supramolecular architecture of **4a**.

UV–Vis spectroscopy

All the studied compounds exhibit broad absorption bands with the maxima at 320–380 nm in 2-MTHF (Table 3 and Figs. 4, 5). The vinylogous enlargement of the conjugation (**1a** → **3a**) results in a bathochromic shift of 19 nm.

While the size of the alkyl group has no effect on the position of the absorption maxima (cf. **3a**, **3c**), the replacement of R¹ by phenyl group results in the bathochromic shift of 20 nm (cf. **3a**, **3b**, Fig. 10 left). The complexation of compounds **3** with triphenyl borane (to give **4**) or boron trifluoride (to give **5**) leads to the large hypsochromic shift of the intense absorption bands (24 nm for **a** and **c**, 34 nm for **b**, and 36 nm for **d**, Fig. 4 right and Fig. 5, Table 3). The hypsochromic shifts could be connected with a decrease of an interaction of the N1 nitrogen with coumarin ring caused by the complexation.

Luminescence

Very weak fluorescence quantum yields ($\Phi < 0.01$) were found for the compounds **3** in 2-MTHF at room temperature. The other compounds do not fluoresce at all in the solution at room temperature. At 77 K a luminescence was detected (Figs. 6 and 7 left).

In the range of 370–500 nm, the compounds **3a–3c** show a fluorescence with well-cut vibronic structure; in comparison with **3a** and **3c**, the fluorescence maxima of **3b** are bathochromically shifted by 40 nm.

All the complexed compounds (**4**, **5**) exhibit broad fluorescence bands with maxima at 465 nm (**4a**, **4c**), 425 nm

(**5a**), and at 422 nm (**5c**); in comparison with the compounds **a** and **c** the fluorescence maxima of compounds **b** are bathochromically shifted by 40–50 nm.

The fluorescence spectra at room temperature show similar trends as do the absorption bands, i.e., significant bathochromic shifts of the compounds **b**.

The compounds **a** and **c**, show a phosphorescence in the range 450–600 nm at 77 K; the phosphorescence spectra of the compounds **3a** and **3c** exhibit a clear cut vibronic structure, while the phosphorescence spectra of the compounds **4a**, **4c** and **5a**, **5c** consist of one broad band. The lifetime of the phosphorescence was found to be very short (20–30 μ s) and may correspond to the emission from a $T_{n\pi^*}$ state. The absence of phosphorescence in all compounds **b** may be due to the bathochromic shift of the absorption band and subsequently by changing the deactivation cascade with respect to the energy of $n\pi^*$ singlet and triplet states.

Because of the very small fluorescence quantum yield, the fluorescence kinetics was measured for highly concentrated solutions. Multi-exponential decay kinetics with time constants in a range of 1–3 ns was observed (Fig. 8). Besides the low-temperature phosphorescence, the relatively long (ns) lifetimes together with low fluorescence quantum yields also imply coupling of the emitting state to the triplet state manifold. If the non-radiative de-excitation were caused by fast internal conversion only, the radiative lifetimes would be unrealistically long.

The fluorescence spectra of the studied compounds in the solid state (powder) are formed by structural bands (compounds **3**) and broad structureless bands (**4** and **5**) with maxima in the range 423–550 nm (Fig. 7 right) With regard to the used experimental techniques (luminescence detected from the surface of pressed powder), only one relation could be detected: the exchange of the phenyl rings

Table 3 Spectral characteristics of the studied compounds

	2-MTHF			Powder
	$\lambda_{A(\max)}/\text{nm}$	$\epsilon/10^3 \text{ mol}^{-1} \text{ dm}^3 \text{ cm}^{-1}$	$\lambda_{F(\max)}/\lambda_{Ph(\max)} (77 \text{ K})/\text{nm}$	$\lambda_{F(\max)}/\text{nm}$
3a	362	37,000	397, 420/499, 538	516, 549
3b	382	31,000	436, 460/–	469, 485
3c	362	39,000	399, 422/496, 537	475, 516
3d	339	27,000	384, 405, 420/–	420
4a	341	43,000	465/540	460
4b	381	71,000	516/–	508
4c	341	48,000	465/531	513
4d	368	40,000	441, 469, 500/–	479
5a	317	30,000	427/510	415
5b	347	11,000	464/–	451
5c	316	29,000	422/498	423
5d	332	20,000	373, 396, 419/–	425

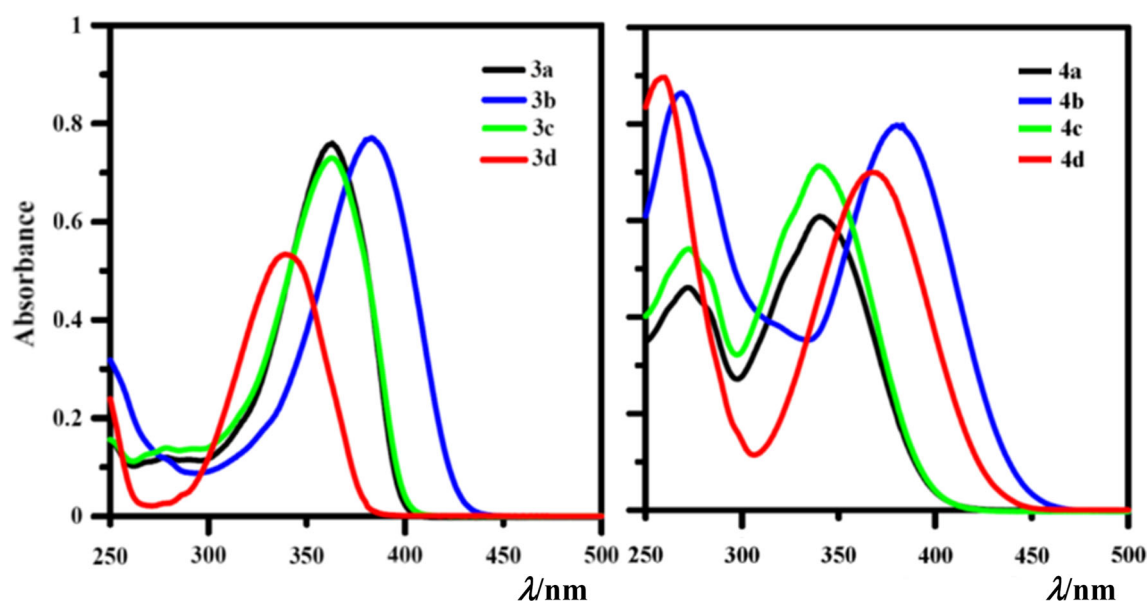


Fig. 4 The absorption spectra of **3a–3d** (left) and **4a–4d** (right) in 2-MTHF

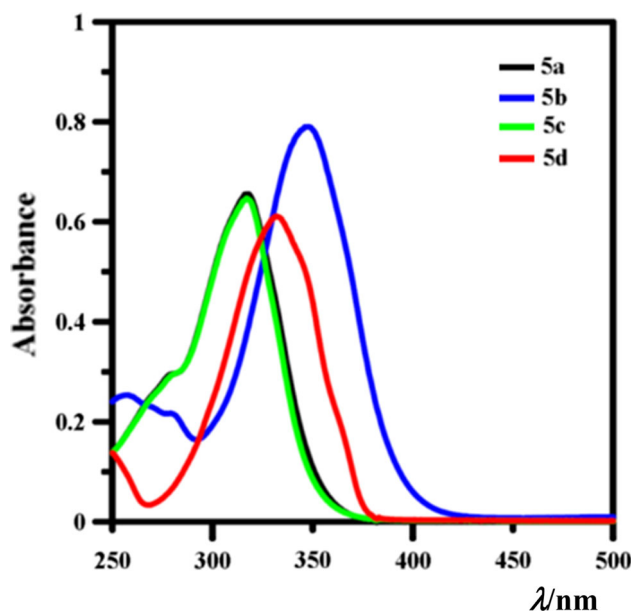


Fig. 5 The absorption spectra of **5a–5d** in 2-MTHF

by the fluorines on the boron atom (**4** → **5**) results in strong hypsochromic shift (45–90 nm). It is noteworthy that the same dependence show the fluorescence spectra in 2-MTHF at 77 K. The spectral characteristics of the compounds **d** as the part of all the studied compounds were also investigated; the absorption spectra are formed by broad bands with maxima at 340–370 nm. At 77 K these compounds exhibit well-structured fluorescence spectra. No phosphorescence was found.

AIE/AIEE properties

From the above-mentioned discussion on the luminescence properties it follows that the compounds studied are solid state luminophores, but their solution state luminescence is poor. Compounds with such behaviour are potential AIE-gens, i.e., exhibit aggregation induced emission (AIE) or aggregation induced emission enhancement (AIEE). This phenomenon is important from the aspect of the application of luminescent materials and has recently been extensively reviewed, see, e.g., [77, 113, 114]. In our previous work [98] we have performed preliminary AIE exploration of boron iminoenolates substituted with *N*-coumarin-6-yl fragment. The samples studied showed to be AIE-active.

Inspired by the previous results [98] we performed similar study also for 7-aminocoumarin analogues. The compounds **3** do not exhibit any AIE properties, but boron complexes **4**, **5** do.

The THF solution of **4a** does not show any fluorescence at room temperature. But in 99% (v/v) water/THF mixture upon excitation at 397 nm, a yellow-green fluorescence appeared. AIE is well documented by the photographs and fluorescence spectra of the solutions with different amount of water (Fig. 9). Practically no AIE was detected for the solution with 80% of water. Compared with absorption spectrum in 2-MTHF (Fig. 10), the excitation spectrum of **4a** in aggregated form is shifted bathochromically about by 60 nm. Very similar AIE characteristics exhibit all derivatives of **4** and **5** (Figs. 9, 10). Similar to the absorption, low-temperature fluorescence and solid state fluorescence spectra, the AIE of compounds **4b** and **5b** is shifted bathochromically by about 50 nm compared to the

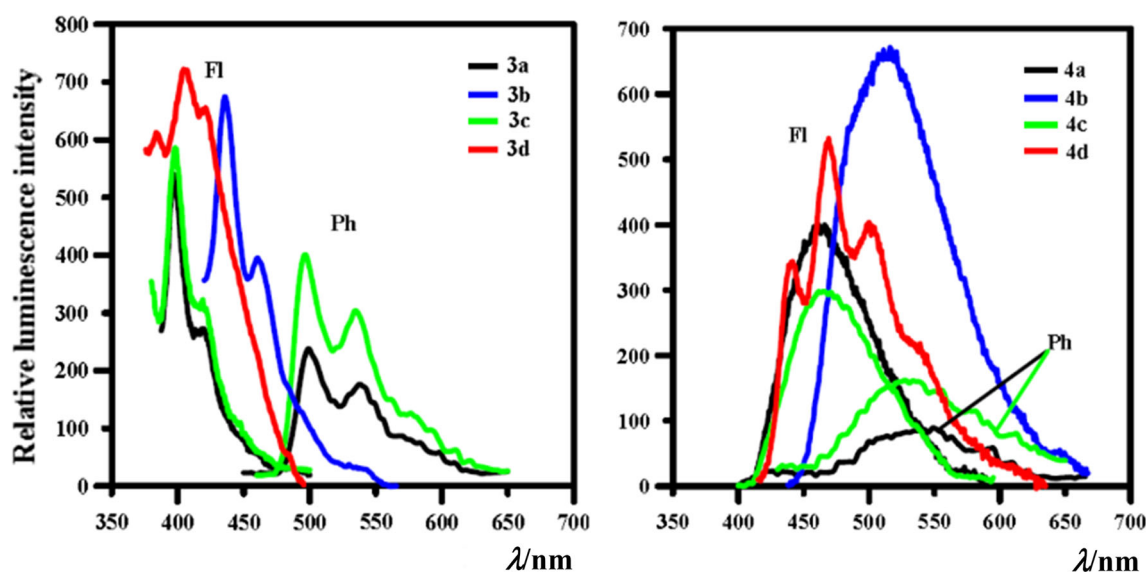


Fig. 6 The luminescence spectra of **3a–3c** (left) and **4a–4d** (right) in 2-MTHF at 77 K

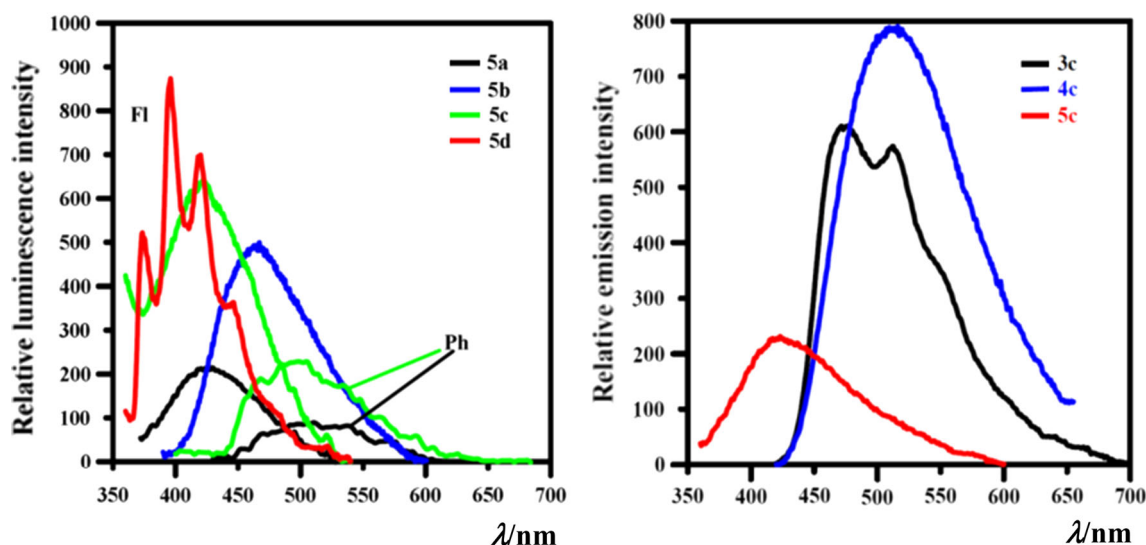


Fig. 7 The luminescence spectra of **5a–5d** (left) in 2-MTHF at 77 K and **3c–5c** (right) in solid state

derivatives **a** and **c**. In comparison with AIE, the fluorescence spectra of the compounds **4** and **5** in solid state (powder) exhibit very similar shapes, but their maxima are shifted hypsochromically about by 50 nm (e.g., compound **5b**, Fig. 10). Compound **4b** was observed to gradually decompose in highly diluted aqueous THF solutions to give aminocoumarin **1a**. This is clearly visible as liberated **1a** gives rise to blue fluorescence whereas pure **4b** in solution does not fluoresce (see Fig. S35). Stability and resulting possible applications of these compounds are to be the subject of further studies. On the other hand, *N*-methyl analogues **4d**, **5d** are not AIEgens as possess no fluorescence even at high concentrations of the poor solvent (99% water in THF).

Theoretical calculations

For deeper insight into UV–Vis absorption properties, the DFT calculations were performed. The energy levels of HOMO and LUMO orbitals are illustrated in Fig. 11.

The results indicate that substitution of phenyl groups (**4**) on the boron atom by fluorine atoms (**5**) leads to decrease of HOMO and LUMO energy levels and increase of HOMO–LUMO energy gap. This is in agreement with observed bathochromic shift of compounds **4**. This could be explained by the fact that in the fluorine-substituted compounds **5**, the HOMO orbitals are distributed mainly over the coumarin and the oxazaborine moiety. However, substitution of fluorine atoms for phenyl groups in

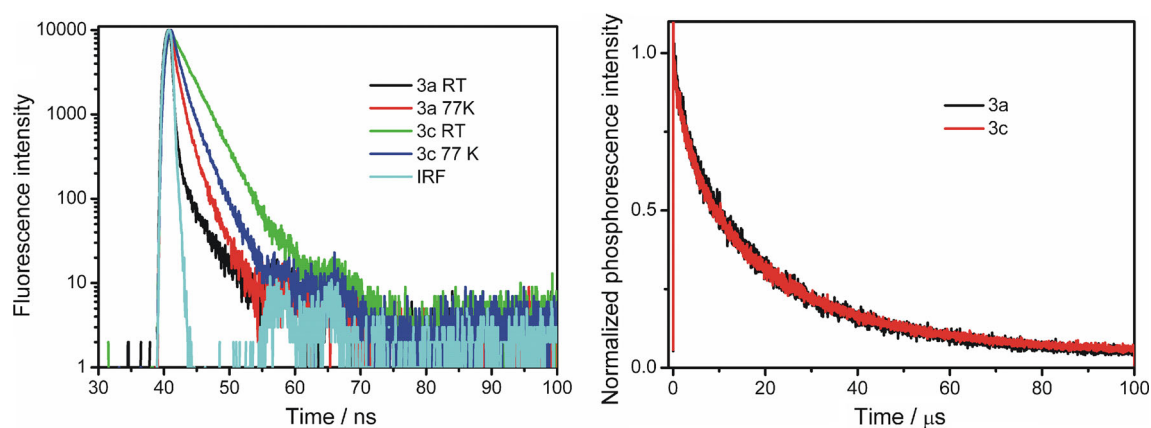


Fig. 8 Fluorescence (left) and phosphorescence (right) decay kinetics of **3a** and **3c** in 2-MTHF. Fluorescence was measured at room temperature and 77 K, phosphorescence only at 77 K

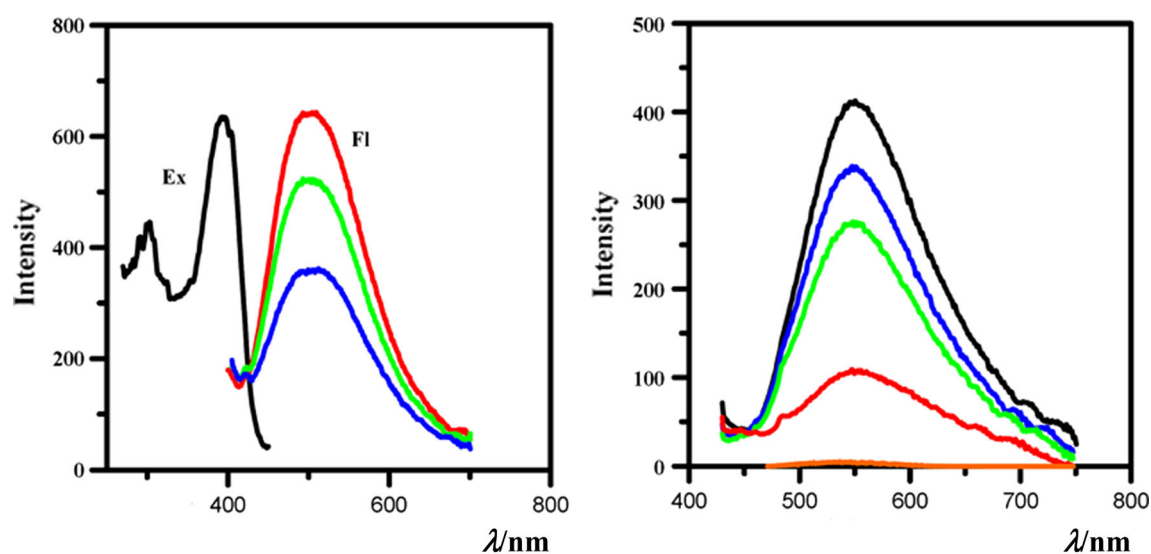


Fig. 9 Left: the aggregate form excitation (Ex) and fluorescence (Fl) spectra of **4a** in H₂O/THF mixtures: 99% (red line), 95% (green line) and 90% (blue line) of water. Right: the aggregate form excitation (Ex) and fluorescence (Fl) spectra of **4b** in H₂O/THF mixtures: 99%

(black line), 95% (blue line), 90% (green line), 80% (red line), and 70% (orange line) of water. Bottom: photographs of **4a** in H₂O/THF mixture (10⁻⁴ M) under UV irradiation ($\lambda = 360$ nm). The amount of water is 0, 50 and 99% (from the left)

compounds **5** causes appearance of new higher energy levels for HOMO orbitals located mainly on these phenyl groups. The bathochromic shift caused by the substitution of methyl (**4a**, **5a**) for phenyl (**4b**, **5b**) in position 6 of the oxazaborine ring could be explained in similar way. The LUMO orbitals in methyl substituted compounds **4a**, **5a** are

located on the oxazaborine and the coumarin moieties. However, in phenyl substituted compounds **4b**, **5b** these LUMOs are distributed on the phenyl instead of the coumarin moieties. The results of TDDFT calculations including λ_{max} , oscillator strength values f and the main orbital transitions are summarized in Table 4. The

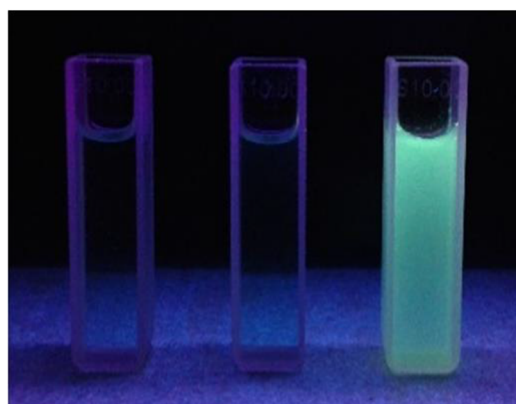
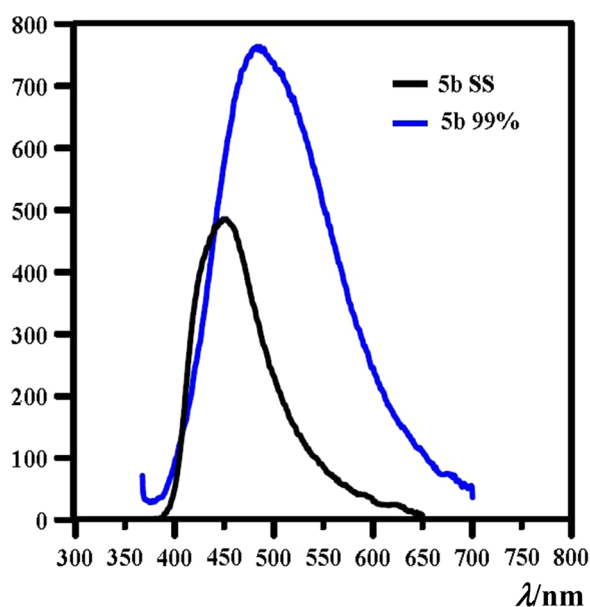


Fig. 10 AIE study of compound **5b**. Left part: photographs of **5b** in H₂O/THF mixture (10⁻⁴ M) under UV irradiation ($\lambda = 360$ nm). The amount of water is 0, 50, and 99% (from the left). Right part:



fluorescence spectrum of **5b** in the aggregated (99% H₂O/THF mixture) and the solid state (SS)

calculated λ_{max} values are in good agreement with the experimental values. Contrary to the work of Kubota [57], the $S_0 \rightarrow S_1$ and $S_0 \rightarrow S_2$ transitions are attributed to the transitions from the HOMO to LUMO and HOMO-1 to LUMO, respectively. Location of HOMO and LUMO orbitals in different parts of compounds **4a**, **4b** and **5a**, **5b** indicates that an intramolecular charge-transfer (ICT) occurs.

Electrochemistry

The fundamental electrochemical characterization of the newly synthesized oxazaborine molecules was performed in acetonitrile containing 0.1 M Bu₄NPF₆ as the supporting electrolyte. To get consistent information, several voltammetric techniques (cyclic voltammetry, rotating disk voltammetry, and polarography) as well as electrode materials: platinum, glassy carbon, mercury (to discern a role of electrode material) were employed. The electrochemical data are summarized in Table 5 and the main attention has been paid to first oxidation and reduction potentials and their reversibility considering that their values are related to HOMO and LUMO energies, moreover their difference reflects HOMO–LUMO gap.

Reduction

The first reduction of compounds **4a–4f** proceeds at potentials of -1.44 to -1.68 V (vs. SCE) as diffusion controlled one-electron (quasi)reversible process with

cathodic/anodic peak separation 76–93 mV. Concerning the substitution on the nitrogen of the oxazaborine core, when comparing methyl substitution (in **4d**) with the coumarin one within the series, the electron-withdrawing effect of the coumarin moiety causes shift of reduction potentials to less positive values. Moreover, there is not big difference in the reduction potentials of the oxazaborines bearing either coumarin-7-yl (**4a**, **4b**) or coumarin-6-yl (**4e**, **4f**). Furthermore, when comparing reduction of **4a** and **4b** where the methyl is replaced by phenyl group, the less positive potential of the latter one is connected to delocalization of electron density as described above in the chapter Theoretical calculations. In the second series **5a–5f** the reduction process follows in similar manner as for **4a–4f**. The main role plays the electron-withdrawing effect of two fluorine substituents which replaced both phenyl groups and caused (e.g., for **5a** in comparison to **4a**) a shift of the first reduction potential by about 100 mV to less positive values.

Oxidation

The first oxidation of compounds **4a–4f** proceeds at potentials of $+1.51$ to $+1.77$ V (vs. SCE) and from comparison of limiting oxidation current from RDV with one-electron reduction current it assumes as a two-electron irreversible process probably of the ECE type. The oxidation most easily proceeds for **4d** whereas the presence of coumarin-7-yl (**4a**, **4b**) or coumarin-6-yl (**4e**, **4f**) moieties increase oxidation potentials by similar manner and their

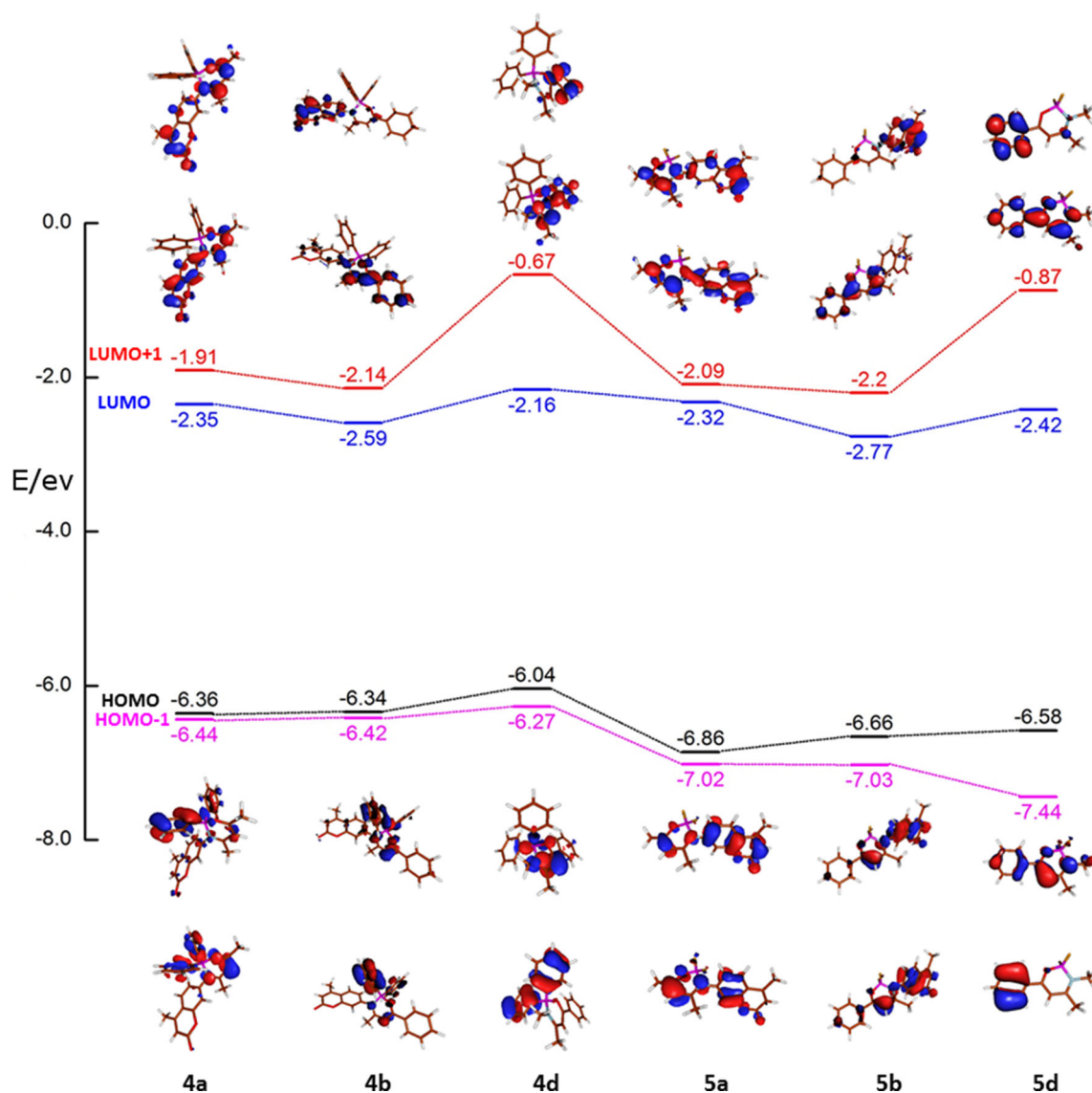


Fig. 11 Molecular orbital energy diagram and isodensity surface (contour value 0.04) plots of the HOMO-1, HOMO, LUMO, and LUMO+1 orbitals

differences can be explained by the above-mentioned displacement of HOMO. The oxidation of compounds **5** is outside the potential window given by electrode, solvent, and supporting electrolyte. For voltammograms see Supporting Information.

Conclusion

Six novel oxazaborines containing 7-aminocoumarin motif were prepared from the corresponding β -enaminones. For an evaluation of the effect of the coumarin fragment, *N*-methyl analogues were synthesized as well. The compounds were characterized by means of ^1H , ^{13}C , ^{11}B , and ^{19}F NMR spectroscopy as well as X-ray diffraction of the

selected compound. Proton and carbon NMR spectroscopy as well as X-ray revealed predominating enol-iminate structure. Molecular dynamics of selected oxazaborines was studied by means of VT NMR (^{19}F , ^1H) and EXSY spectroscopy. The compounds studied exhibit mutual interconversion between R's within the BR_2 fragment. The rate is affected by the substituent on the nitrogen atom. Whereas *N*-methyl compounds **4d**, **5d** possesses fast exchange even at laboratory temperature, the exchange in their coumarin-7-yl derivatives **4a–4c** and **5a–5c** is significantly slower. The absorption spectra of all the studied compounds consist of a single broad, intense band in range 300–400 nm. The complexation of the boron fragment leads to a hypsochromic shift of the absorption maxima apparently due to a decoupling of the nitrogen with the

Table 4 Results of TDDFT calculations at the B3LYP/6-311+G** level of theory and experimentally obtained absorption maxima

	Transition	$\lambda_{A(\max)}/\text{nm calc}$	Main orbital transition	f	$\lambda_{A(\max)}/\text{nm obs}$
4a	S ₀ → S ₁	362	HOMO → LUMO (0.94)	0.05	341
	S ₀ → S ₂	352	HOMO-1 → LUMO (0.95)	0.14	
4b	S ₀ → S ₁	388	HOMO → LUMO (0.91)	0.18	381
	S ₀ → S ₂	379	HOMO-1 → LUMO (0.91)	0.17	
4d	S ₀ → S ₁	370	HOMO → LUMO (0.97)	0.18	368
	S ₀ → S ₂	355	HOMO -1 → LUMO (0.98)	0.01	
5a	S ₀ → S ₁	328	HOMO → LUMO (0.97)	0.37	317
	S ₀ → S ₂	300	HOMO -1 → LUMO (0.79)	0.12	
5b	S ₀ → S ₁	360	HOMO → LUMO (0.98)	0.65	347
	S ₀ → S ₂	325	HOMO -1 → LUMO (0.88)	0.25	
5d	S ₀ → S ₁	321	HOMO → LUMO (0.99)	0.55	332
	S ₀ → S ₂	285	HOMO -1 → LUMO (0.88)	0.02	
6a	S ₀ → S ₁	317	HOMO → LUMO (0.73)	0.17	307
	S ₀ → S ₂	310	HOMO → LUMO + 1 (0.75)	0.04	
6b	S ₀ → S ₁	347	HOMO → LUMO (0.92)	0.47	343
	S ₀ → S ₂	323	HOMO → LUMO +1 (0.94)	0.03	
7a	S ₀ → S ₁	351	HOMO → LUMO (0.91)	0.01	334
	S ₀ → S ₂	343	HOMO -1 → LUMO (0.93)	0.01	
7b	S ₀ → S ₁	374	HOMO → LUMO (0.56)	0.09	377
	S ₀ → S ₂	370	HOMO -1 → LUMO (0.58)	0.15	

Table 5 Electrochemical data of studied compounds

	$E_{1/2}(\text{ox1})/\text{V}$	$E_{1/2}(\text{red1})/\text{V}$	$E_{\text{ox}} - E_{\text{red},a}/\text{V}$
4a	1.77	- 1.68	3.45
4b	1.67	- 1.44	3.11
4d	1.51	- 1.81	3.33
4e	1.77	- 1.66	3.42
4f	1.68	- 1.56	3.23
5a	-	- 1.58	-
5b	-	- 1.31	-
5d	-	- 1.63	-
5e	-	- 1.63	-
5f	-	- 1.43	-

coumarin ring. In a solution, none of the studied compounds fluoresce at room temperature. In 2-MTHF at 77 K, the compounds **3** exhibit a fluorescence with a clear cut vibronic structure while the fluorescence of **3b** is more bathochromically shifted. The complexation (compounds **4** and **5**) leads to a significant bathochromic shift of fluorescence formed by a single broad band. Compounds **3a**, **3c** show a phosphorescence with a well-cut vibronic structure; the phosphorescence of **4a**, **4c** and **5a**, **5c** consist of a single broad, bathochromically shifted, band. Compounds **b** do not phosphoresce. The lifetime of the phosphorescence was found to be 20–30 μs and may correspond to the emission

from a $T_{n\pi^*}$ state. Compounds **d** exhibit only a fluorescence with a clear cut vibronic structure; no phosphorescence was detected. In comparison with the derivatives of 6-aminocoumarin, the derivatives of 7-aminocoumarin exhibit higher luminescence intensities in solid, frozen solution, and aggregated states as well. Simultaneously the phosphorescence spectra of some derivatives of 7-aminocoumarin are shifted bathochromically compared to the fluorescence spectra. This fact has given us the possibility of further investigation of photophysical properties of these compounds, i.e., fluorescence and phosphorescence lifetime. The AIE tests in THF/water mixture showed that compounds **4**, **5** are AIE-active molecules. The change of the substituent on the nitrogen (compounds **4d**, **5d**) led to complete inhibition of AIE properties. Concerning the electrochemical properties, the first reduction of all compounds **4** and **5** proceeds as transport controlled one-electron (quasi)reversible process at potentials of - 1.31 to - 1.81 V (vs. SCE). It was observed that the reduction potential is significantly influenced by substituents on the nitrogen of the oxazaborine core. The electron-withdrawing ability of either coumarin-7-yl (**4a**, **4b**) or coumarin-6-yl (**4e**, **4f**) cause shift of reduction potential from 130 to 370 mV to less positive values in comparison to methyl substitution. Moreover, two fluorine substituents which replaced both phenyl groups (in, e.g., **5a**) shifted the first reduction potential by another 100 mV in the same direction in comparison to **4a**. The first oxidation of oxazaborines **4a–4f** proceeds as a two-electron irreversible

process at potentials of + 1.51 to + 1.77 V (vs. SCE), most probably of the ECE type and is again influenced by coumarin-7-yl or coumarin-6-yl moieties. The oxidation of compounds **5** was not possible to obtain within the given potential window. Analysis of frontier orbitals showed that substitution of fluorine atoms in **5** to phenyl groups on the boron atom (giving compounds **4**) leads to decrease of energy gap that explains observed bathochromic shift. The same applies to substitution of methyl (**4a**, **5a**) to phenyl (**4b**, **5b**) in position 6 of the oxazaborine ring.

Experimental

NMR spectra were measured using NMR spectrometers Bruker AVANCE III operating at 400.13 MHz (^1H), 376.50 MHz (^{19}F), 127.38 MHz (^{11}B), and 100.12 MHz (^{13}C) and Bruker AscendTM equipped with CryoprobeTM Prodigy operating at 500.13 MHz (^1H), 470.66 MHz (^{19}F), 160.48 (^{11}B), and 125.12 MHz (^{13}C). Proton spectra in CDCl_3 were calibrated on internal TMS ($\delta = 0.00$ ppm) and in $\text{DMSO}-d_6$ on the middle peak of the solvent multiplet ($\delta = 2.50$ ppm). Carbon spectra were measured with broadband proton decoupling in an ordinary way or using APT pulse sequence. Calibration of the carbon spectra was done on the middle peak of the solvent multiplet ($\delta = 77.23$ ppm in CDCl_3 and 39.51 in $\text{DMSO}-d_6$). Fluorine-19 NMR spectra were measured without proton decoupling using α,α,α -trifluorotoluene as the secondary external standard ($\delta = -63.9$ ppm against CFCl_3 as the primary standard) [115]. Boron-11 NMR were measured in 5 mm quartz NMR tubes (Norell) using $\text{B}(\text{OMe})_3$ as an external standard ($\delta = 18.1$ ppm) [116]. All the pulse sequences were taken from the Bruker pulse sequence library. The multiplicity of the signals is expressed as follows: s (singlet), d (doublet), t (triplet), q (quartet), dd (doublet of doublets), m (multiplet), br (broadened signal).

The X-ray data for colourless crystals of **4a** were obtained at 150 K using Oxford Cryostream low-temperature device on a Nonius Kappa CCD diffractometer with $\text{Mo K}\alpha$ radiation ($\lambda = 0.71073$ Å), a graphite monochromator, and the ϕ and χ scan mode. Data reductions were performed with DENZO-SMN [117]. The absorption was corrected by integration methods [118]. Structures were solved by direct methods (Sir92) [119] and refined by full matrix least-square based on F^2 (SHELXL97) [120]. Hydrogen atoms were mostly localized on a Fourier difference electron density map, however, to ensure uniformity of treatment of the crystal, all hydrogen atoms were recalculated into idealized positions (riding model) and assigned temperature factors $H_{\text{iso}}(\text{H}) = 1.2 U_{\text{eq}}$ (pivot atom) or $1.5 U_{\text{eq}}$ (methyl). Hydrogen atoms in methyl

moieties and in aromatic rings were placed with C–H distances of 0.96 and 0.93 Å, respectively.

$$\begin{aligned} R_{\text{int}} &= \sum |F_o^2 - F_{o,\text{mean}}^2| / \sum F_o^2, \text{ GOF} \\ &= [\sum (w(F_o^2 - F_c^2)^2) / (N_{\text{diffrs}} \\ &\quad - N_{\text{params}})]^{1/2} \text{ for all data, } R(F) \\ &= \sum ||F_o| - |F_c|| / \sum |F_o| \text{ for observed data, } wR(F^2) \\ &= [\sum (w(F_o^2 - F_c^2)^2) / (\sum w(F_o^2)^2)]^{1/2} \text{ for all data.} \end{aligned}$$

Crystallographic data for structural analysis have been deposited with the Cambridge Crystallographic Data Centre, CCDC no. 1413238 for **4a**. Copies of this information may be obtained free of charge from The Director, CCDC, 12 Union Road, Cambridge CB2 1EY, UK (fax: +44-1223-336033; e-mail: deposit@ccdc.cam.ac.uk or www: <http://www.ccdc.cam.ac.uk>). Crystal data for **4a** are in Supplement together with other characterization data.

The absorption spectra were measured on a UV/Vis Perkin-Elmer Lambda 35 spectrophotometer at room temperature. The emission spectra were measured on a Perkin-Elmer LS55 Spectrofluorimeter equipped with a commercial low-temperature accessory and a special commercial cuvette. For fluorescence measurements, the solutions of very low concentration about 10^{-6} mol dm^{-3} (optical density ~ 0.05 at the excitation wavelength in 1-cm cell) were used. The fluorescence spectra in solid phase were recorded from the surface of the pressed powder in the special cuvette. The spectra were corrected for the characteristics of the emission monochromator and for the photomultiplier response and by excitation at the wavelengths of the absorption maxima. The luminescence kinetics was measured using Horiba Jobin–Yvon Fluoromax TCSPC spectrometer. The cylindrical round-bottom quartz cuvette with the solution was placed into the Oxford Research Instrument OPTISTAT^{DN} cryostat. As the excitation source, 370 nm IBH NanoLED was used. Fluorescence decay kinetics at 296 K was recorded at 430 nm (4 nm bandwidth) using 1 MHz excitation pulse repetition rate. Phosphorescence decay kinetics at 77 K was measured at 537 nm (14 nm bandwidth) using 1 kHz repetition rate.

Electrochemical measurements were carried out in acetonitrile containing 0.1 M Bu_4NPF_6 . Cyclic voltammetry (CV), rotating disk voltammetry (RDV), and polarography were used in a three-electrode arrangement. The working electrode was glassy carbon or platinum disk (2 mm in diameter) for CV and RDV experiments, whereas for the study of reduction a dropping mercury electrode (DME) was employed. As the reference and auxiliary electrodes were used saturated calomel electrodes (SCE) separated by a bridge filled with supporting electrolyte. All potentials are given vs. SCE. Voltammetric measurements

were performed using a potentiostat PGSTAT 128 N (AUTOLAB, Metrohm Autolab B.V., Utrecht, The Netherlands) operated via NOVA 1.11 software.

The calculations were performed using the density functional method B3LYP (Refs. [121–124]) in conjunction with 6-31+G** basis set as implemented in the Gaussian 09 suite [125]. For all optimized structures, frequency analyses at the same level of theory were used to assign them as genuine minima on the potential energy surface. The single point and TDDFT calculations were performed on the optimized structures on the B3LYP/6-311+G** level of theory.

All the solvents and reagents were commercial and used without further treatment.

General procedure for the synthesis of β -enaminones **3a–3c**

The mixture of 1.2 g 7-amino-4-methylcoumarin (**1a**, 6.85 mmol), β -diketone **2a–2c** (6.85 mmol, 8.63 mmol in the case of **2a**), and catalytic amount of *p*-toluenesulfonic acid (10 mg, 0.058 mmol) in 80 cm³ toluene was refluxed for 18–20 h. Water formed during the reaction was azeotropically distilled off. The solvent was evaporated under reduced pressure. The crude products **3a–3c** (white or yellow solids) were purified by recrystallization or isolated by column chromatography.

4-Methyl-7-[[[(2Z)-4-oxopent-2-en-2-yl]amino]-2H-chromen-2-one (3a, C₁₅H₁₅NO₃) From 7-amino-4-methylcoumarin (**1a**) and acetylacetone (**2a**). Reaction time 20 h. Recrystallization from ethanol afforded 0.65 g (37%) of yellow solid. M.p.: 165–166.5 °C; ¹H NMR (500 MHz, CDCl₃): δ = 12.73 (br s, 1H), 7.54 (d, *J* = 8.5 Hz, 1H), 7.08 (d, *J* = 2.2 Hz, 1H), 7.00 (dd, *J* = 8.5 Hz, *J* = 2.2 Hz, 1H), 6.23 (br q, *J* = 1.2 Hz, 1H), 5.30 (s, 1H), 2.43 (d, *J* = 1.3 Hz, 3H), 2.17 (s, 3H), 2.14 (s, 3H) ppm; ¹³C NMR (125 MHz, CDCl₃): δ = 197.6, 161.0, 158.2, 154.4, 152.3, 142.6, 125.6, 119.4, 116.5, 113.8, 110.2, 100.4, 29.7, 20.7, 18.8 ppm.

7-[(2Z)-(4-Oxo-4-phenylbut-2-en-2-yl)amino]-4-methyl-2H-chromen-2-on (3b, C₂₀H₁₇NO₃) From 7-amino-4-methylcoumarin (**1a**) and benzoylacetone (**2b**). Reaction time 18 h. Repeated column chromatography (CHCl₃:EtOAc 3:2; DCM:EtOAc 10:1) afforded 1.31 g (60%) of yellow solid. M.p.: 160–160.5 °C; ¹H NMR (400 MHz, CDCl₃): δ = 13.36 (br s, 1H), 7.93–7.91 (m, 2H), 7.57 (d, *J* = 8.5 Hz, 1H), 7.52–7.43 (m, 3H), 7.14 (d, *J* = 2.1 Hz, 1H), 7.09 (dd, *J* = 8.5 Hz, *J* = 2.2 Hz, 1H), 6.23 (br q, *J* = 1.1 Hz, 1H), 5.99 (br s, 1H), 2.43 (d, *J* = 1.1 Hz, 3H), 2.31 (s, 3H) ppm; ¹³C NMR (100 MHz, CDCl₃): δ = 189.7, 160.9, 160.2, 154.4, 152.2, 142.5, 139.6, 131.7,

128.6, 127.4, 125.6, 119.5, 116.8, 113.9, 110.4, 96.8, 21.3, 18.8 ppm.

4-Methyl-7-[[[(3Z)-5-oxohept-3-en-3-yl]amino]-2H-chromen-2-one (3c, C₁₇H₁₉NO₃) From 7-amino-4-methylcoumarin (**1a**) and heptane-3,5-dione (**2c**). Reaction time 18 h. Column chromatography (silica gel/CHCl₃-EtOAc 3:2 v/v) furnished 1.17 g of pale yellow solid. M.p.: 101–102.5 °C; ¹H NMR (500 MHz, CDCl₃): δ = 12.74 (br s, 1H), 7.54 (d, *J* = 8.5 Hz, 1H), 7.07 (d, *J* = 2.2 Hz, 1H), 7.01 (dd, *J* = 8.5 Hz, *J* = 2.2 Hz, 1H), 6.23 (br q, *J* = 1.2 Hz, 1H), 5.33 (s, 1H), 2.50 (q, *J* = 7.4 Hz, 2H), 2.45–2.41 (m, 5H), 1.17–1.14 (m, 6H) ppm; ¹³C NMR (125 MHz, CDCl₃): δ = 201.6, 163.7, 161.1, 154.5, 152.3, 142.7, 125.6, 119.6, 116.5, 113.8, 110.7, 97.4, 35.7, 25.7, 18.8, 12.6, 9.7 ppm.

General procedure for the synthesis of oxazaborines **4a–4d**

The flask fitted with a calcium chloride drying tube was charged with enaminone **3a–3d** (2 mmol) in 20 cm³ anhydrous DCM. Afterwards 0.6 g triphenylborane (2.5 mmol) was added gradually under argon atmosphere. The reaction mixture was then stirred for 2–7 days at room temperature. The crude product was isolated by column chromatography followed by further purification (see details at individual compounds).

4,6-Dimethyl-2,2-diphenyl-3-(4-methyl-2-oxo-2H-chromen-7-yl)-1,3,2λ⁴-oxazaborine (4a, C₂₇H₂₄BNO₃) From **3a**, reaction time 6 days. Volatile components were evaporated in vacuo and ca. 10 cm³ MeOH was added to the residue. The flask with the mixture was immersed into an ultrasonic bath. The precipitate formed was isolated by suction. Recrystallization from EtOH afforded 0.25 g (40%) of white solid. M.p.: 217.5–218.5 °C; ¹H NMR (500 MHz, CDCl₃): δ = 7.31–7.28 (m, 5H), 7.18–7.13 (m, 6H), 6.88 (d, *J* = 1.9 Hz, 1H), 6.73 (dd, *J* = 8.3 Hz, *J* = 1.9 Hz, 1H), 6.21 (br q, *J* = 1.3 Hz, 1H), 5.48 (s, 1H), 2.32 (d, *J* = 1.2 Hz, 3H), 2.09 (s, 3H), 2.00 (s, 3H) ppm; ¹³C NMR (125 MHz, CDCl₃): δ = 180.2, 169.1, 160.6, 153.4, 152.0, 146.4, 133.7–133.5 (br), 127.1–126.9 (br), 126.6–126.3 (br), 124.7, 123.2, 118.6, 115.8, 115.2, 100.8, 23.8, 22.3, 18.8 ppm.

4-Methyl-3-(4-methyl-2-oxo-2H-chromen-7-yl)-2,2,6-triphenyl-1,3,2λ⁴-oxazaborine (4b, C₃₂H₂₆BNO₃) From **3b**, reaction time 6 days. Volatile components were subsequently evaporated in vacuo and the residue was subjected to column chromatography [silica gel, CHCl₃:EtOAc (3:2 v/v)]. Subsequent recrystallization from EtOH afforded 0.23 g (85%) of white solid. M.p.: 203.5–205 °C; ¹H NMR (400 MHz, CDCl₃): δ = 7.95–7.92 (m, 2H), 7.51–7.47 (m,

1H), 7.43–7.37 (m, 6H), 7.31 (d, $J = 8.5$ Hz, 1H), 7.18–7.12 (m, 6H), 6.96 (d, $J = 2$ Hz, 1H), 6.80 (dd, $J = 8.4$ Hz, $J = 2.2$ Hz, 1H), 6.22 (br q, $J = 1.2$ Hz, 1H), 6.18 (s, 1H), 2.33 (d, $J = 1.1$ Hz, 3H), 2.15 (s, 3H) ppm; ^{13}C NMR (100 MHz, CDCl_3): $\delta = 173.3, 169.7, 160.6, 153.5, 151.9, 146.6, 134.3, 133.7$ (br), 132.4, 128.7, 127.9, 127.0 (br), 126.5 (br), 124.7, 123.2, 118.7, 115.8, 115.3, 97.7, 22.9, 18.8 ppm.

4,6-Diethyl-3-(4-methyl-2-oxo-2H-chromen-7-yl)-2,2-diphenyl-1,3,2 λ^4 -oxazaborine (4c, C₂₉H₂₈BNO₃) From **3c**, reaction time 6 days. Volatile components were evaporated in vacuo and ca. 10 cm³ MeOH was added to the residue. The flask with the mixture was immersed into an ultrasonic bath. The precipitate formed was isolated by suction. Recrystallization from EtOH afforded 0.34 g (44%) of yellow solid. M.p.: 168–169 °C; ^1H NMR (500 MHz, CDCl_3): $\delta = 7.30$ –7.26 (m, 5H), 7.15–7.11 (m, 6H), 6.89 (d, $J = 2.0$ Hz, 1H), 6.73 (dd, $J = 8.4$ Hz, $J = 2.0$ Hz, 1H), 6.21 (br q, $J = 1.2$ Hz, 1H), 5.51 (s, 1H), 2.35–2.32 (m, 5H), 2.27 (q, $J = 7.6$ Hz, 2H), 1.17 (t, $J = 7.5$ Hz, 3H), 1.11 (t, $J = 7.5$ Hz, 3H) ppm; ^{13}C NMR (125 MHz, CDCl_3): $\delta = 184.5, 174.0, 160.6, 153.4, 152.0, 146.1, 133.7, 133.5, 127.0, 126.8, 126.5, 126.2, 124.6, 123.4, 118.5, 115.9, 115.2, 97.2, 30.4, 28.0, 18.8, 12.6, 10.6$ ppm.

3,4-Dimethyl-2,2,6-triphenyl-1,3,2 λ^4 -oxazaborine (4d, C₂₃H₂₂BNO) From **3d**, reaction time 6 days. Volatile components were evaporated and the residue was subjected to column chromatography [silica gel, CHCl_3 :EtOAc (3:2 v/v)]. Subsequent recrystallization from EtOH afforded 1.0 g (86%) of yellow solid. M.p.: 174–176 °C; ^1H NMR (400 MHz, CDCl_3): $\delta = 7.87$ –7.85 (m, 2H), 7.43–7.32 (m, 7H), 7.28–7.18 (m, 6H), 5.84 (s, 1H), 2.93 (s, 3H), 2.17 (s, 3H) ppm; ^{13}C NMR (100 MHz, CDCl_3): $\delta = 170.2, 168.9, 148.9$ (br), 134.8, 133.2, 131.4, 128.5, 127.3, 127.2, 126.4, 96.6, 37.4, 21.2 ppm.

General procedure for the synthesis of oxazaborines 5a–5d

The procedure was adopted from Ref. [126]. Enaminone **3a–3d** (1.5 mmol) was dissolved in 10 cm³ DCM and 0.42 cm³ triethylamine (3 mmol) was added afterwards. The reaction mixture was stirred at room temperature for 20 min. Consequently, 1.16 cm³ 48% $\text{BF}_3 \cdot \text{Et}_2\text{O}$ (4.5 mmol) was added; the mixture was refluxed for 3 h and then stirred for another 12–87 h at room temperature. The crude product was obtained by evaporation of the solvent and further purified.

2,2-Difluoro-4,6-dimethyl-3-(4-methyl-2-oxo-2H-chromen-7-yl)-1,3,2 λ^4 -oxazaborine (5a, C₁₅H₁₄BF₂NO₃) From **3a**,

stirred for 87 h at room temperature; the volatile components were evaporated under reduced pressure; the residue was suspended in water. The product was isolated by suction; recrystallization from ethanol followed with washing with ether afforded 0.22 g (46%) of white solid. M.p.: 195.5–196.5 °C; ^1H NMR (500 MHz, CDCl_3): $\delta = 7.69$ –7.67 (m, 1H), 7.21–7.20 (m, 2H), 6.34 (br q, $J = 1.2$ Hz, 1H), 5.61 (s, 1H), 2.46 (d, $J = 1.3$ Hz, 3H), 2.23 (s, 3H), 2.01 (s, 3H) ppm; ^{13}C NMR (125 MHz, CDCl_3): $\delta = 178.8, 171.7, 160.3, 153.9, 151.9, 142.7, 125.8, 122.6, 120.0, 115.8, 115.5, 99.3, 23.3, 21.6, 18.9$ ppm; HRMS (MALDI): C₁₅H₁₄BF₂NO₃ requires $[\text{M} + \text{H}]^+$ 306.11076, found 306.11076; $[\text{M} + \text{Na}]^+$ 328.09270, found 328.09270; $[\text{M} - \text{F}]^+$ 286.10453, found 286.10392.

2,2-Difluoro-4-methyl-6-phenyl-3-(4-methyl-2-oxo-2H-chromen-7-yl)-1,3,2 λ^4 -oxazaborine (5b, C₂₀H₁₆BF₂NO₃) From **3b**, stirred for 12 h at room temperature, the volatile components were evaporated in vacuo, the residue was purified by washing with ether and ethanol. Yield 0.83 g (90%) of light yellow solid. M.p.: 266–267.5 °C; ^1H NMR (400 MHz, CDCl_3): $\delta = 8.01$ –7.99 (m, 2H), 7.72–7.69 (m, 1H), 7.59–7.55 (m, 1H), 7.51–7.47 (m, 2H), 7.28–7.26 (m, 2H), 6.35 (br q, $J = 1.2$ Hz, 1H), 6.28 (s, 1H), 2.47 (d, $J = 1.2$ Hz, 3H), 2.16 (s, 3H) ppm; ^{13}C NMR (100 MHz, CDCl_3): $\delta = 172.3, 171.9, 160.3, 154.0, 151.9, 142.9, 133.1, 133.0, 129.0, 127.9, 125.8, 122.6, 120.1, 115.9, 115.5, 96.1, 22.2, 18.9$ ppm; HRMS (MALDI): C₂₀H₁₆BF₂NO₃ requires $[\text{M} + \text{H}]^+$ 368.12641, found 368.12697; $[\text{M} + \text{Na}]^+$ 390.10835, found 390.10902; $[\text{M} - \text{F}]^+$ 348.12018, found 348.12068.

4,6-Diethyl-2,2-difluoro-3-(4-methyl-2-oxo-2H-chromen-7-yl)-1,3,2 λ^4 -oxazaborine (5c, C₁₇H₁₈BF₂NO₃) From **3c**, stirred for 12 h at room temperature. Column chromatography [silica gel, CHCl_3 :EtOAc (3:2 v/v)] afforded 0.54 g (96%) of white solid. M.p.: 130–131 °C; ^1H NMR (500 MHz, CDCl_3): $\delta = 7.69$ –7.67 (1H, m), 7.22–7.20 (2H, m), 6.34 (1H, br q, $J = 1.3$ Hz), 5.63 (1H, s), 2.50 (2H, q, $J = 7.6$ Hz), 2.46 (3H, d, $J = 1.2$ Hz), 2.27 (2H, q, $J = 7.6$ Hz), 1.26 (3H, t, $J = 7.5$ Hz), 1.13 (3H, t, $J = 7.6$ Hz) ppm; ^{13}C NMR (125 MHz, CDCl_3): $\delta = 183.3, 176.4, 160.4, 153.9, 151.9, 142.4, 125.7, 122.9, 120.0, 115.8, 115.7, 95.7, 30.1, 27.4, 18.9, 12.2, 10.6$ ppm; HRMS (MALDI): C₁₇H₁₈BF₂NO₃ requires $[\text{M} + \text{H}]^+$ 334.14206, found 334.14248; $[\text{M} + \text{Na}]^+$ 356.12400, found 356.12450; $[\text{M} - \text{F}]^+$ 314.13583, found 314.13620.

2,2-Difluoro-3,4-dimethyl-6-phenyl-1,3,2 λ^4 -oxazaborine (5d, C₁₁H₁₂BF₂NO) Synthesis and structure of these compounds were described previously in Ref. [100]. From **3d**, reaction time 20 h, the precipitate was filtered off and the filtrate was evaporated in vacuo. Recrystallization from

ethanol afforded 0.4 g (53%) of white solid. M.p.: 138–139 °C; ^1H NMR (400 MHz, $\text{DMSO-}d_6$): δ = 7.93–7.91 (m, 2H), 7.59–7.49 (m, 3H), 6.52 (s, 1H), 3.16 (s, 3H), 2.35 (s, 3H) ppm; ^{13}C NMR (100 MHz, $\text{DMSO-}d_6$): δ = 173.0, 166.0, 132.0, 128.9, 126.6, 96.1, 32.5, 20.2 ppm; HRMS (MALDI): $\text{C}_{11}\text{H}_{12}\text{BF}_2\text{NO}$ requires $[\text{M} + \text{Na}]^+$ 246.08722, found 246.08755; $[\text{M} + \text{K}]^+$ 262.06154, found 262.06116; $[\text{M} - \text{F}]^+$ 204.09905, found 204.09918.

Acknowledgements HD and PŠ would like to thank the Faculty of Chemical Technology, University of Pardubice for the institutional support.

References

- Liu X, Xu Z, Cole JM (2013) *J Phys Chem C* 117:16584
- Grandberg II, Denisov LK, Popova OA (1987) *Chem Heterocycl Compd* 23:117
- Lakowicz JR (2006) *Principles of fluorescence spectroscopy*, 3rd edn. Springer, Berlin
- Christie RM, Lui C-H (2000) *Dyes Pigment* 47:79
- Trenor SR, Shultz AR, Love BJ, Long TE (2004) *Chem Rev* 104:3059
- Wheelock CE (1959) *J Am Chem Soc* 81:1348
- Kitamura N, Fukagawa T, Kohtani S, Kitoh S, Kunimoto K-K, Nakagaki R (2007) *J Photochem Photobiol A* 188:378
- Nakagaki R, Kitamura N, Aoyama I, Ohtsubo H (1994) *J Photochem Photobiol A* 80:113
- Reddy AR, Prasad DV, Darbarwar M (1986) *J Photochem* 32:69
- Kuznetsova NA, Kaliya OL (1992) *Russ Chem Rev* 61:1243
- Donovalová J, Cigáň M, Stankovičová H, Gaplovsky A (2012) *Molecules* 17:3259
- Atkins RL, Bliss DE (1978) *J Org Chem* 43:1975
- Christie RM, Lui C-H (1999) *Dyes Pigment* 42:85
- Lin Q, Du Z, Yang Y, Fang Q, Bao C, Yang Y, Zhu L (2014) *Chem Eur J* 20:16314
- Lin Q, Bao C, Cheng S, Yang Y, Ji W, Zhu Y (2012) *J Am Chem Soc* 134:5052
- Wu J, Kwon B, Liu W, Anslyn EV, Wang P, Kim JS (2015) *Chem Rev* 115:7893
- Sabnis RW (2015) *Handbook of fluorescent dyes and probes*. Wiley, Hoboken
- Christie RM (2001) *Colour chemistry*. RSC, Cambridge
- Silfvast WT (2004) *Laser fundamentals*, 2nd edn. Cambridge University Press, Cambridge
- Thiel E (2000) *Laser Dyes*. In: Elvers B (ed) *Ullmann's encyclopedia of industrial chemistry*. Wiley, Weinheim, p 323
- Clark M (2011) *Handbook of textile and industrial dyeing*, vol 1. Woodhead Publishing, Sawston
- Christie RM, Morgan KM, Islam MS (2008) *Dyes Pigment* 76:741
- Sumiya S, Shiraishi Y, Hirai T (2013) *J Phys Chem A* 117:1474
- Li G, Zhu D, Liu Q, Xue L, Jiang H (2013) *Org Lett* 15:2002
- Chemate S, Sekar N (2015) *J Fluoresc* 25:1615
- Jin X, Uttamapinant C, Ting AY (2011) *ChemBioChem* 12:65
- Gonçalves MST (2009) *Chem Rev* 109:190
- Lim S-Y, Na M-J, Kim H-J (2013) *Sens Actuators B* 185:720
- Li H, Cai L, Chen Z (2012) *Coumarin-derived fluorescent chemosensors*. In: Wang W (ed) *Advances in chemical sensors*. InTech, p 121
- Haugland RP (2002) *Handbook of fluorescent probes and research products*, 9th edn. Molecular Probes Inc, Eugene
- Li J, Zhang C-F, Yang S-H, Yang W-C, Yang G-F (2014) *Anal Chem* 86:3037
- Wirtz L, Auerbach D, Jung G, Kazmaier U (2012) *Synthesis* 44:2005
- de Silva AP, Gunaratne HQN, Gunnlaugsson T, Huxley AJM, McCoy CP, Rademacher JT, Rice TE (1997) *Chem Rev* 97:1515
- Lavis LD, Raines RT (2008) *ACS Chem Biol* 3:142
- Corrie JET, Munasinghe VRN, Rettig W (2000) *J Heterocycl Chem* 37:1447
- Arbeloa TL, Arbeloa FL, Arbeloa IL (1996) *J Lumin* 68:149
- Park S-Y, Ebihara M, Kubota Y, Funabiki K, Matsui M (2009) *Dyes Pigment* 82:258
- Liu X, Cole JM, Waddell PG, Lin T-C, McKechnie S (2013) *J Phys Chem C* 117:14130
- Liu X, Cole JM, Waddell PG, Lin T-C, Radia J, Zeidler A (2012) *J Phys Chem A* 116:727
- Kubota Y, Hara H, Tanaka S, Funabiki K, Matsui M (2011) *Org Lett* 13:6544
- Josefík F, Svobodová M, Bertolasi V, Šimůnek P, Macháček V, Almonasy N, Černošková E (2012) *J Organomet Chem* 699:75
- Yoshii R, Tanaka K, Chujo Y (2014) *Macromolecules* 47:2268
- Kumbhar HS, Gadilohar BL, Shankarling GS (2015) *Spectrochim Acta A* 146:80
- Fedorenko EV, Tretyakova GO, Mirochnik AG, Beloliptsev AY, Svistunova IV, Sazhnikov VA, Atabekyan LS (2016) *J Fluoresc* 26:1839
- Grabarz AM, Jędrzejewska B, Zakrzewska A, Zalesny R, Laurent AD, Lacquemin D, Osmialowski B (2017) *J Org Chem* 82:1529
- Tanaka K, Chujo Y (2015) *NPG Asia Mater* 7:e223
- Kubota Y, Kasatani K, Niwa T, Sato H, Funabiki K, Matsui M (2016) *Chem Eur J* 22:1816
- Zhou L, Xu D, Gao H, Han A, Liu X, Zhang C, Li Z, Yang Y (2017) *Dyes Pigment* 137:200
- Zhou L, Xu D, Gao H, Han A, Yang Y, Zhang C, Liu X, Zhao F (2016) *RSC Adv* 6:69560
- Yoshii R, Suenaga K, Tanaka K, Chujo Y (2015) *Chem Eur J* 21:7231
- Frath D, Azizi S, Ulrich G, Ziessel R (2012) *Org Lett* 14:4774
- Macedo FP, Gwengo C, Lindeman SV, Smith MD, Gardinier JD (2008) *Eur J Inorg Chem* 4:3200
- Wesela-Bauman G, Urban M, Lulinski S, Serwatowski J, Wozniak K (2015) *Org Biomol Chem* 13:3268
- Murale DP, Lee KM, Kim K, Churchill DG (2011) *Chem Commun* 47:12512
- Frath D, Azizi S, Ulrich G, Retailleau P, Ziessel R (2011) *Org Lett* 13:3414
- Koyama Y, Matsumura T, Yui T, Ishitani O, Takata T (2013) *Org Lett* 15:4686
- Kubota Y, Sakuma Y, Funabiki K, Matsui M (2014) *J Phys Chem A* 118:8717
- Liao C-W, Rao RM, Sun S-S (2015) *Chem Commun* 51:2656
- Kumbhar HS, Shankarling GS (2015) *Dyes Pigment* 122:85
- Wu Y, Li Z, Liu Q, Wang X, Yan H, Gong S, Liu Z, He W (2015) *Org Biomol Chem* 13:5775
- Dai C, Yang D, Fu X, Chen Q, Zhu C, Cheng Y, Wang L (2015) *Polym Chem* 6:5070
- Dai C, Yang D, Zhang W, Fu X, Chen Q, Zhu C, Cheng Y, Wang L (2015) *J Mater Chem B* 3:7030
- Matsumura T, Koyama Y, Uchida S, Yonekawa M, Yui T, Ishitani O, Takata T (2014) *Polym J* 46:609
- Suenaga K, Yoshii R, Tanaka K, Chujo Y (2015) *Macromol Chem Phys* 217:414

65. Yang Z, Jiang B, Hao W-J, Zhou P, Tu S-J, Li G (2015) *Chem Commun* 51:1267
66. Wei H, Wang G, Wang Y, Li B, Huang J, Kashtanov S, van Hecke K, Pereshivko OP, Peshkov VA (2017) *Chem Asian J* 12:825
67. Fedorenko EV, Mirochnik AG, Beloliptsev AY, Svistunova IV, Tretyakova GO (2018) *ChemPlusChem* 83:117
68. Tolle N, Dunkel U, Oehninger L, Ott I, Preu L, Haase T, Behrends S, Jones PG, Totzke F, Schaechtele C, Kubbutat MHG, Kunick C (2011) *Synthesis* 2011:2848
69. Xia M, Wu B, Xiang G (2008) *J Fluor Chem* 129:402
70. Yoshii R, Nagai A, Tanaka K, Chujo Y (2013) *Chem Eur J* 19:4506
71. Zyabrev K, Dekhtyar M, Vlasenko Y, Chernega A, Slominskii Y, Tolmachev A (2012) *Dyes Pigment* 92:749
72. Jiang X, Liu X, Jiang Y, Quan Y, Cheng Y, Zhu C (2014) *Macromol Chem Phys* 215:358
73. Yoshii R, Nagai A, Tanaka K, Chujo Y (2014) *Macromol Rapid Commun* 35:1315
74. Suenaga K, Tanaka K, Chujo Y (2016) *Chem Eur J* 23:1409
75. Gao H, Xu D, Liu X, Han A, Zhou L, Zhang C, Yang Y, Li W (2017) *RSC Adv* 7:1348
76. Zhang P, Liu W, Niu G, Xiao H, Wang M, Ge J, Wu J, Zhang H, Li Y, Wang P (2017) *J Org Chem* 82:3456
77. Mei J, Leung NLC, Kwok RTK, Lam JWY, Tang BZ (2015) *Chem Rev* 115:11718
78. Yang H, Ye K, Sun J, Gong P, Lu R (2017) *Asian J Org Chem* 6:199
79. Zhao J, Peng J, Chen P, Wang H, Xue P, Lu R (2018) *Dyes Pigment* 149:276
80. Nosova EV, Moshkina TN, Lipunova GN, Baklanova IV, Slepukhin PA, Charushin VN (2015) *J Fluor Chem* 175:145
81. Hachiya S, Inagaki T, Hashizume D, Maki S, Niwa H, Hirano T (2010) *Tetrahedron Lett* 51:1613
82. Hachiya S, Hashizume D, Ikeda H, Yamaji M, Maki S, Niwa H, Hirano T (2016) *J Photochem Photobiol A* 331:206
83. Suenaga K, Tanaka K, Chujo Y (2017) *Eur J Org Chem* 2017:5191
84. Qi F, Lin J, Wang X, Cui P, Yan H, Gong S, Ma C, Liu Z, Huang W (2016) *Dalton Trans* 45:7278
85. Yao Q-C, Wu D-E, Ma R-Z, Xia M (2013) *J Organomet Chem* 743:1
86. Gao H, Xu D, Wang Y, Zhang C, Yang Y, Liu X, Han A, Wang Y (2018) *Dyes Pigment* 150:165
87. Zakrzewska A, Kolehmainen E, Valkonen A, Haapaniemi E, Rissanen K, Chęcińska L, Ośmiałowski B (2013) *J Phys Chem A* 117:252
88. Ośmiałowski B, Zakrzewska A, Jędrzejewska B, Grabarz A, Zaleśny R, Bartkowiak W, Kolehmainen E (2015) *J Org Chem* 80:2072
89. Grabarz AM, Laurent AD, Jędrzejewska B, Zakrzewska A, Jacquemin D, Ośmiałowski B (2016) *J Org Chem* 81:2280
90. Kubota Y, Ozaki Y, Funabiki K, Matsui M (2013) *J Org Chem* 78:7058
91. Bally I, Ciornei E, Vasilescu A, Balaban AT (1973) *Tetrahedron* 29:3185
92. Rodríguez M, Ramos-Ortíz G, Alcalá-Salas MI, Maldonado JL, López-Varela KA, López Y, Domínguez O, Meneses-Nava MA, Barbosa-García O, Santillan R, Farfán N (2010) *Dyes Pigment* 87:76
93. Singh YP, Rupani P, Singh A, Rai AK, Mehrotra RC, Rogers RD, Atwood JL (1986) *Inorg Chem* 25:3076
94. Yan W, Hong C, Long G, Yang Y, Liu Z, Bian Z, Chen Y, Huang C (2014) *Dyes Pigment* 106:197
95. Pešková M, Šimůnek P, Bertolasi V, Macháček V, Lyčka A (2006) *Organometallics* 25:2025
96. Svobodová M, Bárta J, Šimůnek P, Bertolasi V, Macháček V (2009) *J Organomet Chem* 694:63
97. Svobodová M, Šimůnek P, Macháček V, Štruncová L, Růžička A (2012) *Tetrahedron* 68:2052
98. Doušová H, Šimůnek P, Almonasy N, Růžičková Z (2016) *J Organomet Chem* 802:60
99. Rettig W, Klock A (1985) *Can J Chem* 63:1649
100. Itoh K, Okazaki K, Fujimoto M (2003) *Aust J Chem* 56:1209
101. Itoh K, Okazaki K, Chow Y (2004) *Helv Chim Acta* 87:292
102. Itoh K, Okazaki K, Sera A, Chow YL (1992) *Chem Commun* 1992:1608
103. Itoh K, Fujimoto M, Hashimoto M (2002) *New J Chem* 26:1070
104. Eaton GR (1969) *J Chem Educ* 46:547
105. Lee D, Newman SG, Taylor MS (2009) *Org Lett* 11:5486
106. Sachdev H, Zahn N, Huch V (2009) *Z Anorg Allg Chem* 635:2112
107. Šimůnek P, Svobodová M, Bertolasi V, Pretto L, Lyčka A, Macháček V (2007) *New J Chem* 31:429
108. Chatterjee A, Chakrabarti R, Das B, Kanrar S, Banerji J, Budzikiewicz H, Neuman A, Prange T (1992) *Heterocycles* 34:259
109. Lugo AF, Richards AF (2010) *Eur J Inorg Chem* 2010:2025
110. Kuo P-C, Chen I-C, Lee HM, Hung CH, Huang J-H (2005) *Inorg Chim Acta* 358:3761
111. Wang S, Zhao Y, Zhao C, Liu L, Yu SJ (2013) *J Fluor Chem* 156:236
112. Pyykkö P, Atsumi M (2009) *Chem Eur J* 15:186
113. Mei J, Hong Y, Lam JWY, Qin A, Tang Y, Tang BZ (2014) *Adv Mater* 26:5429
114. Hong Y, Lam JWY, Tang BZ (2011) *Chem Soc Rev* 40:5361
115. Berger S, Braun S, Kalinowski H-O (1997) *NMR spectroscopy of the non-metallic elements*. Wiley, Chichester, p 400
116. Kennedy JD (1987) Boron. In: Mason J (ed) *Multinuclear NMR*. Plenum Press, New York, p 221
117. Otwinowski Z, Minor W (1997) *Macromol Crystallogr Pt A* 276:307
118. Coppens P (1970) In: Ahmed FR, Hall SR, Huber CP (eds) *Crystallographic computing*. Munksgaard, Copenhagen, p 255
119. Altomare A, Casciarano G, Giacovazzo C, Guagliardi A (1994) *J Appl Crystallogr* 27:1045
120. Sheldrick GM (2008) *SHELXL-97*. University of Göttingen, Germany
121. Vosko SH, Wilk L, Nusair M (1980) *Can J Phys* 58:1200
122. Lee C, Yang W, Parr RG (1988) *Phys Rev B* 37:785
123. Miehllich B, Savin A, Stoll H, Preuss H (1989) *Chem Phys Lett* 157:200
124. Becke AD (1993) *J Chem Phys* 98:5648
125. Frisch MJ, Trucks GW, Schlegel HB, Scuseria GE, Robb MA, Cheeseman JR, Scalmani G, Barone V, Mennucci B, Petersson GA, Nakatsuji H, Caricato M, Li X, Hratchian HP, Izmaylov AF, Bloino J, Zheng G, Sonnenberg JL, Hada M, Ehara M, Toyota K, Fukuda R, Hasegawa J, Ishida M, Nakajima T, Honda Y, Kitao O, Nakai H, Vreven T, Montgomery JA Jr, Peralta JE, Ogliaro F, Bearpark M, Heyd JJ, Brothers E, Kudin KN, Staroverov VN, Kobayashi R, Normand J, Raghavachari K, Rendell A, Burant JC, Iyengar SS, Tomasi J, Cossi M, Rega N, Millam JM, Klene M, Knox JE, Cross JB, Bakken V, Adamo C, Jaramillo J, Gomperts R, Stratmann RE, Yazyev O, Austin AJ, Cammi R, Pomelli C, Ochterski JW, Martin RL, Morokuma K, Zakrzewski VG, Voth GA, Salvador P, Dannenberg JJ, Dapprich S, Daniels AD, Farkas O, Foresman JB, Ortiz JV, Cioslowski J, Fox DJ (2009) *Gaussian 09*, revision D01. Gaussian Inc, Wallingford
126. Ma R-Z, Yao Q-C, Yang X, Xia M (2012) *J Fluor Chem* 137:93